DOI: 10.13009/EUCASS2023-903
Aerospace Europe Conference 2023 – 10TH EUCASS – 9TH CEAS

Aeropropulsive Assessment of the Scramjet Hypersonic Experimental Vehicle

Pietro Roncioni[1] †, Marco Marini[1], Sara Di Benedetto[1], M. Albano[2], R. Bertacin[2]
[1] CIRA Italian Aerospace Research Centre, 81043 Capua, Italy
[2] ASI, Agenzia Spaziale Italiana, 00133 Rome, Italy
p.roncioni@cira.it, m.marini@cira.it, s.dibenedetto@cira.it
marta.albano@asi.it, roberto.bertacin@asi.it
† Corresponding Author

Abstract
The present paper deals with the aerodynamic and propulsive (aeropropulsive) characterization of the Scramjet Hypersonic Experimental Vehicle (SHEV) as part of a research project on experimentation for hypersonic flight and enabling technologies for future high-speed transportation systems. The vehicle SHEV is a propelled hypersonic aircraft in-flight demonstrator posing the challenge of creating, at national level, an aircraft capable of supporting a levelled hypersonic flight thanks to the introduction of a scramjet propulsion system.

1. Introduction

The activities of present paper are part of the research program aimed to develop a national hypersonic vehicles and technologies. The project is focused on experimentation for hypersonic flight, aimed at design, develop and testing the enabling technologies for future high-speed transport systems, with the main objective of design and testing a propelled hypersonic aircraft demonstrator in flight. Despite the numerous initiatives born in Europe in the last 15 years dedicated to hypersonic flight for passenger transport (LAPCAT I&II, ATLLAS I&II, FAST20XX, HIKARI, HEXAFLY, HEXAFLY-INT, STRATOFLY) none of them brought to the testing in flight of a propelled vehicle. The national initiatives that led to the design of prototypes such as, among others, the French aircraft ZEHST, developed by MBDA, ASTRIUM and ONERA, or the English SKYLON by Reaction Engines Ltd., which despite being more oriented towards supersonic flight and access to space, respectively, already include many of the technologies necessary for hypersonic flight. Hypersonic civil transport has always had as its weak point the low cruising autonomy, essentially linked to too high fuel consumption. In recent years, a highly integrated design approach between efficient propulsion systems and high-lift configurations (LAPCAT-II and STRATOFLY configurations) is enabling the trend to be reversed ([1], [2], [4], [4]).
The study on the Scramjet Hypersonic Experimental Vehicle (SHEV) starts from the experience gained thanks to the strong involvement of Italian companies, and CIRA in particular, in the European project HEXAFLY-INT (realization of a flight test of an aircraft without engine for hypersonic flight), and previously in the HEXAFLY one, posing the challenge of creating, at national level, an aircraft capable of supporting a levelled hypersonic flight thanks to the introduction of a scramjet propulsion system.
The project is co-funded by the national research programme PRORA and the Italian Space Agency (ASI), with the aim of designing a hypersonic propelled demonstrator capable of performing a levelled and controlled flight at Mach 6÷8 and an altitude of 28÷32 km, in order to realize and test the enabling technologies for future civil transport systems at hypersonic speed.
This paper deals with activities that aim to verify the aerodynamic efficiency (L/D = 3÷4) and the aeropropulsive balance (T>D) at Mach = 6÷8 in controlled flight. For the purpose of verifying the above requirements, experimental flight conditions falling within the required Mach and altitude ranges were considered. Numerical viscous CFD simulations were conducted both in fuel-off conditions, thus providing us with the values of aerodynamic efficiency and mass flow of air at the combustor inlet (input for the sizing of the tanks and supply lines), and in fuel-on conditions for the verification of the aeropropulsive balance (T>D). Several reacting air-hydrogen mixture schemes have been considered at the same asymptotic conditions for the assessment of the Thrust-Drag balance. In addition, a number of CFD viscous simulations along a preliminary flight trajectory after scramjet engine shutdown (gliding phase down to Mach=2) were also performed to provide full inputs to thermal and flight mechanics analyses.

DOI: 10.13009/EUCASS2023-903

2. Mission and Demonstrator Description

The preliminary mission concept envisages an air-launched solution with a carrier (stage I) capable of releasing the payload, that is as a set of propelled hypersonic demonstrator and launch vehicle equipped with a booster, at a target point in terms of speed and altitude.
From here the launch vehicle accelerates until it reaches the foreseen trajectory target point and releases the hypersonic propelled demonstrator at the experimental window (altitude and Mach objective) where the scramjet must work for a time of at least 10 seconds.
The main phases of an "Air-Launched" mission scenario are (see also Figure 1):

1. Take-off of the carrier aircraft from a civil or military airport
2. Subsonic flight in the direction of the test area
3. Acceleration up to Mach and altitude of separation from the carrier aircraft (transonic or low supersonic, depends on the mother aircraft)
4. Separation of the payload (launch aircraft + demonstrator) from the carrier aircraft and ignition of the booster (sep1)
5. Acceleration from separation Mach to target Mach (6÷8) and target altitude (27÷32 km)
6. Switch off the booster and optimize separation conditions
7. Separation of the propelled hypersonic demonstrator from the launch aircraft (sep2)
8. Ignition and adjustment of the scramjet thruster in the experimental window
9. Scramjet engine shutdown
10. Gliding phase (controlled only aerodynamically) of deceleration of the aircraft
11. Loss of controllability up to Splash Down

It is therefore possible to identify three mission phases:

M1. Step 0: from the release of the payload from the carrier to the release of the demonstrator at the target point (points 4-7 of the previous list);
M2. Step 1: Experimental window (points 8-9 of the previous list);
M3. Step 2: Gliding (points 10-11 of the previous list).

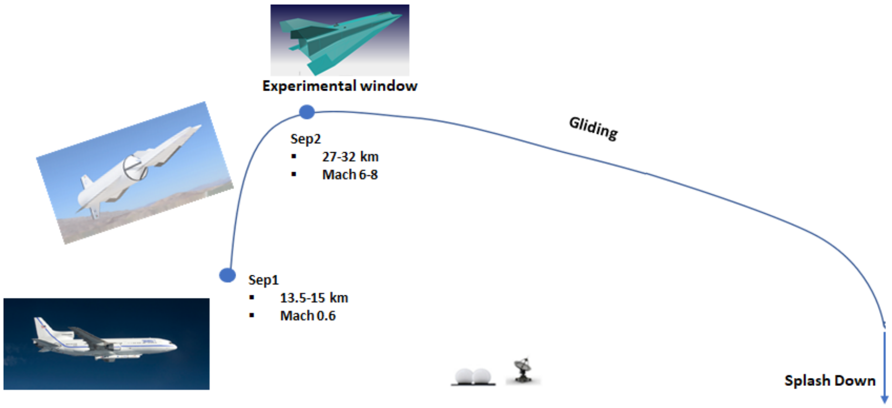

Figure 1: Mission Scenario

The launch mission is the result of a trade-off and feasibility assessment that considered and analysed two possible mission scenarios: launch from a carrier aircraft (airdrop) and launch from the ground with an expendable launcher. The assessment considered both technical aspects, specific to the differ mission profiles and trajectories, and programmatic constraints concerning the availability of carriers/launchers compatible with the mission requirements in terms of performances and planning.
Data from a generic civil aircraft were considered for the present study. This choice will not preclude the use of other carriers, as the launch phase is considered exclusively as a boundary condition for the design of the demonstrator. The launch vehicle connected to the propelled hypersonic demonstrator is represented in Figure 2.

DOI: 10.13009/EUCASS2023-903

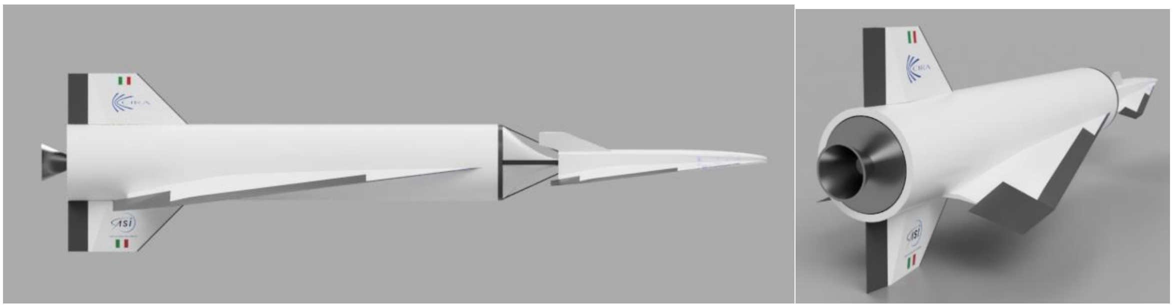

Figure 2: Demonstrator connected to the launch vehicle.

The configuration of the propelled hypersonic demonstrator is based on the concept of "waverider", or a hypersonic vehicle with high aerodynamic efficiency in supersonic regime obtained through the exploitation of shock waves that form on the lifting surfaces, a phenomenon known as "compression lift". The demonstrator must also include a scramjet air-breathing propulsion system. For this concept, particular consideration was given to the configuration studied in the EU-FP7 HEXAFLY (see refs [5], [6], [7]) and depicted in Figure 3:

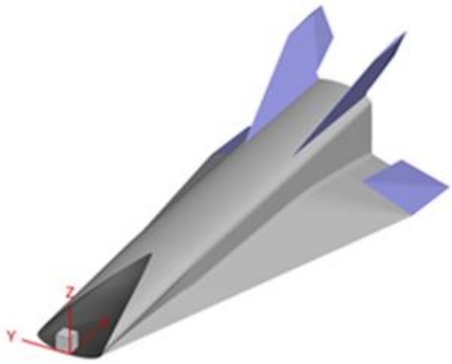

Figure 3: Configuration of the HEXAFLY project demonstrator.

3. AEDB Building

The AErodynamic Data Base (AEDB) Building is the overall procedure that allows to obtain a full and integral set of information and/or data that characterize the aerodynamic environment in terms of flow field features, global and local forces and pressure distributions over the vehicle surfaces.

In particular, the main parameters to be defined are:

- Components of aerodynamic forces and moments versus the main variables characterizing the flight, i.e., Mach and Reynolds numbers, angle of attack, angle of sideslip, deflection of control surfaces, etc…
- Uncertainties levels to be added to the previous nominal data.
- Pressure distributions.

These data are inputs for several disciplines as flight mechanics, thermo-structural analysis, but also in some cases for propulsive database building.

The final and reliable aerodynamic database is foreseen to be obtained by means of both numerical and experimental activities.

In this paper the starting activities results are reported, that are:

- Aero-propulsive Balance and Aerodynamic Efficiency assessment.
- Numerical aerodynamic database built by means of CFD simulations.

DOI: 10.13009/EUCASS2023-903

4. Aero-Propulsive Balance and Aerodynamic Efficiency

The verification of the aeropropulsive balance and aerodynamic efficiency in cruise conditions is presented in this paragraph. For this purpose, two flight conditions falling within the required Mach and altitude ranges were considered below (see Table 1).

Table 1: Matrix test for hypersonic cruise conditions

Altitude	H = 27 km	H = 31.9 km
Static pressure p_∞	1828 Pa	875.5 Pa
Static temperature T_∞	222.3 K	235.97 K
Static density ρ_∞	0.02852 kg/m3	0.01293 kg/m3
Mach number M_∞	7.350	7.355
Flow velocity u_∞	2202 m/s	2264.7 m/s
MFR	**4.851 kg/s**	**2.246 kg/s**

Numerical CFD viscous simulations were conducted with the ANSYS FLUENT® CFD code on a grid of 7.6 million cells (Figure 4) and with the boundary conditions shown in Figure 5.

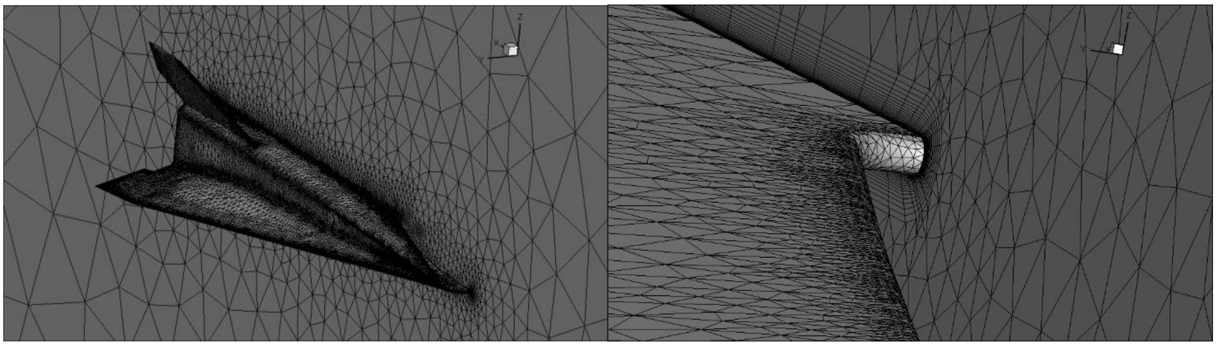

Figure 4: Calculation grid for simulations with the engine on.

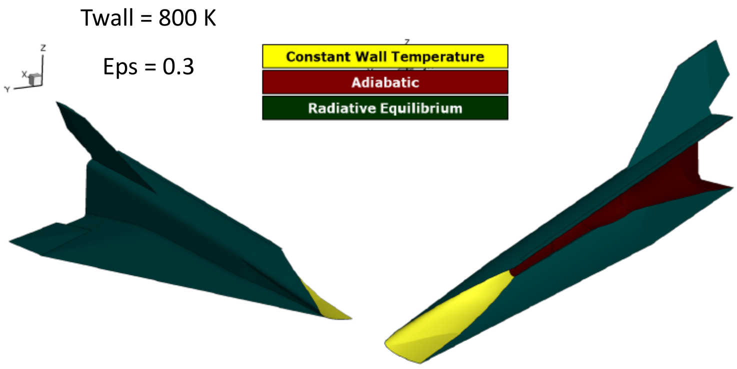

Figure 5: Applied thermal boundary conditions.

The initial simulations conducted with the engine off settings (Fuel-off) provided us with the values of aerodynamic efficiency and mass flow of air at the combustor inlet. This last value served as input for the sizing of the tanks and supply lines, an activity conducted by the propulsion unit.
Table 2 summarizes the aerodynamic parameters of interest. The values were extracted by distinguishing the external part (fuselage, wings and empennages) and the internal part composed of air intake, combustor and nozzle. The flight experiment takes place in motor-on conditions, and in these conditions for the purposes of aerodynamic efficiency only the external part of the aircraft is considered, this is because the whole internal duct acts as an engine and has a positive thrust such as to balance the resistance of the remaining part of the aircraft (external part). In such conditions the total resistance is zero. From the table you can see how the efficiency E_{ext} (external) is well above 4 (almost 5). It will be seen later that this value is also confirmed in motor-on conditions.
In addition, from the table it is possible to see that even the total efficiency E_{tot}, which makes sense as argued above for the motor-off conditions that occur after the shutdown of the scramjet, is well within the mission requirements (value around 3.5).

DOI: 10.13009/EUCASS2023-903

Table 2: Summary of aerodynamic parameters of cruising with the engine off

H	Mach	Type	CL_ext	CL_int	CL_tot	CD_ext	CD_int	CD_tot	CM_ext	CM_int	CM_tot	E_ext	E_int	E_tot
27.00	7.350	No-Inj	0.04004	0.001299	0.041339	0.008267	0.00336	0.01163	-0.02362	-0.00304	-0.02667	4.8431	0.3865	3.5552
31.90	7.355	No-Inj	0.03996	0.001166	0.041130	0.008604	0.00345	0.01205	-0.02355	-0.00296	-0.0265	4.6449	0.3380	3.4125

Following the verification of the aerodynamic efficiency requirement, it was then necessary to verify the aeropropulsive balance. This expression means that the thrust delivered by the scramjet engine must be verified to counterbalance the aerodynamic drag of the external part of the aircraft. Before this assessment it is necessary to verify that the balance of the internal path alone is first verified, that is, the engine starts and the gross thrust of the "thrust chamber" (combustor + nozzle) is at least able to overcome the drag of the intake (very high in hypersonic conditions). The net thrust, i.e. the gross thrust decreased by the drag of the air intake (which is considered to be part of the engine), must therefore be greater than or equal to the external drag.
Simulations with air-hydrogen reacting flow were therefore conducted under the same asymptotic conditions as in Table 1. For the fuel injection, two front semi-struts have been provided, positioned at the beginning of the combustion chamber and on both sides of the same, and a rear full-strut positioned further downstream and laying on the symmetry plane (see Figure 6). Each semi-strut is provided with a single injection hole positioned on the top, whereas the full strut is equipped with four injection holes positioned on the sides and rear.

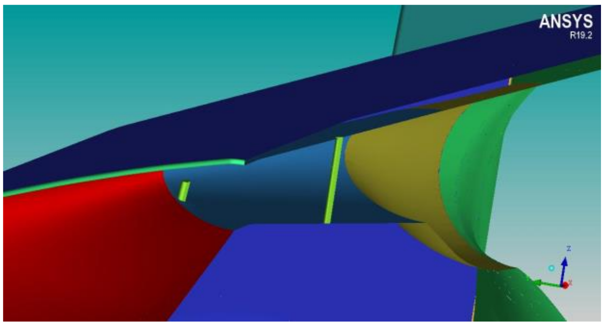

Figure 6: Positioning of semi-strut and strut in combustion chamber (half aircraft).

Starting from the mass flow data of air entering the combustion chamber and setting the hydrogen-air equivalence ratio (ER: Equivalence Ratio), it is then possible to calculate the mass flow rate of hydrogen to be introduced into the chamber. In the present simulations we considered an ER equal to 1 (stoichiometric proportions) which corresponds to a ratio of hydrogen/air flow rates equal to 0.02924; this flow rate of H_2 was divided between semi-struts and full strut with the following ratios: 0.65 and 0.35. Table 3 reports the details of fuel injection.

Table 3: Fuel inlet parameters (half configuration).

H	Mach FF	MFR air	ER	MFR H2	M des	Struts	Ptot	Pexit	Mexit
[km]	[-]	[kg/sec]	[-]	[kg/sec]	[-]		[Pa]	[Pa]	[-]
27.00	7.350	2.4255585	1.00	0.0709233	2.00	semi (1)	5510165	704224	1.9927
					2.00	full (2)	9020220	1152825	3.0454
31.90	7.355	1.1227676	1.00	0.0328297	2.00	semi (1)	5643204	721227	2.0000
					2.00	full (2)	3490761	446135	2.0000

In order not to weigh down the numerical calculations too much, a single-step chemical scheme for modelling air-hydrogen combustion was used that considers the only reaction between oxygen and hydrogen, with nitrogen that remains inert and unchanged along the entire internal duct, according to the following scheme:

$$2H_2 + O_2 + 79/21\ N_2 \rightarrow 2H_2O + 79/21N_2$$

From which it is possible to derive stoichiometric mass ratios

$$\frac{\dot{m_{air}}}{\dot{m_{fuel}}} = \frac{\frac{79}{21} * 28 + 1 * 32}{2 * 2} = \frac{2884}{84} = 34.2;\ \frac{\dot{m_{fuel}}}{\dot{m_{air}}} = 0.02924$$

Below is also the definition of Equivalence Ratio:

DOI: 10.13009/EUCASS2023-903

$$\varphi = ER = \frac{\left(\frac{\dot{m}_{fuel}}{\dot{m}_{air}}\right)_{actual}}{\left(\frac{\dot{m}_{fuel}}{\dot{m}_{air}}\right)_{stoich}}$$

In the following figures (Figure 7 and Figure 8) you can see the temperature and water vapor distributions within the propulsive duct. It can be seen that the reaction takes place along the entire propulsive duct (combustion chamber + nozzle). In fact, from past experiences (LAPCAT-II, STRATOFLY) it has been seen that the combustion of hydrogen in similar conditions requires a length of about 2÷3 meters to take place completely. One of the purposes of these reacting simulations was just to verify that combustion takes place satisfactorily.

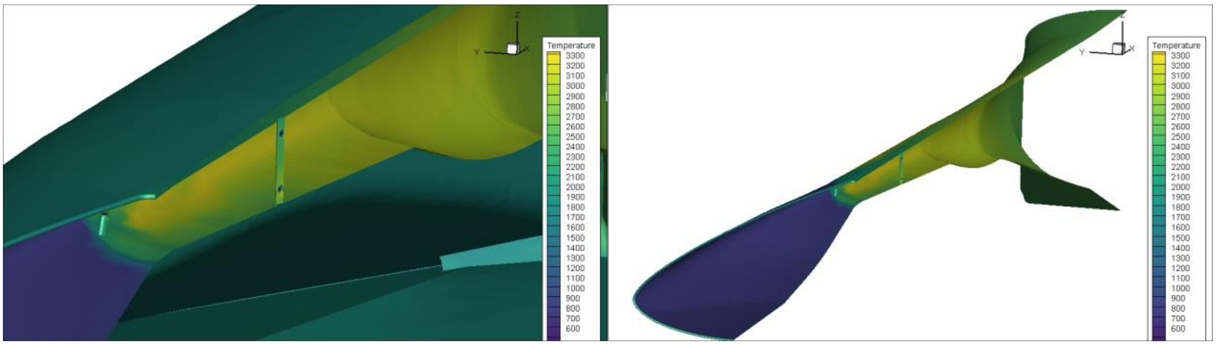

Figure 7: Temperature distributions on the inner walls of the propulsive duct.

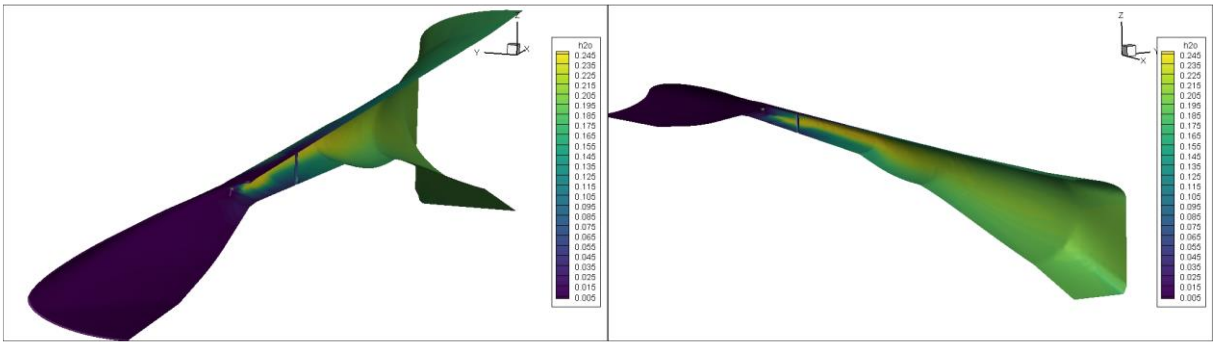

Figure 8: Distribution of water vapor inside the propulsion duct.

Table 4 shows the main results in terms of aerodynamic coefficients for both motor-off (already reported above) and motor-on conditions. First of all, it can be noted that the aero-propulsive balance requirement is met at both altitudes. In fact, the total CD_tot resistance (external + internal) is negative, which means that the thrust of the scramjet engine (C_{thrust} = $-CD_{int}$) is higher than the external resistance (CD_{ext}). Also, from the same table it can be seen that the aerodynamic efficiency values (E_{ext}) remain essentially unchanged compared to the corresponding motor-off cases and largely satisfying the relative mission requirement. Finally, Table 5 shows the aero-propulsive balance in quantitative terms, too.

Table 4: Summary of aerodynamic parameters for cruising with both engine on and off.

H	Mach	Type	CL_ext	CL_int	CL_tot	CD_ext	CD_int	CD_tot	CM_ext	CM_int	CM_tot	E_ext	E_int	E_tot
27.00	7.350	React	0.04032	0.001298	0.041618	0.008509	-0.00915	-0.00064	-0.02380	-0.00295	-0.02675	4.7386	-0.1418	-64.8527
31.90	7.355	React	0.03885	0.002026	0.040875	0.008539	-0.00868	-0.00015	-0.02295	-0.00306	-0.02601	4.5498	-0.2334	-281.5156
27.00	7.350	No-Inj	0.04004	0.001299	0.041339	0.008267	0.00336	0.01163	-0.02362	-0.00304	-0.02667	4.8431	0.3865	3.5552
31.90	7.355	No-Inj	0.03996	0.001166	0.041130	0.008604	0.00345	0.01205	-0.02355	-0.00296	-0.0265	4.6449	0.3380	3.4125

DOI: 10.13009/EUCASS2023-903

Table 5: Summary of axial forces acting on the hypersonic propelled demonstrator.

		Ext	Int	Tot
Forces (N)	27 km	2820	-3032	-213
Mot-on	31.9 km	1357	-1380	-23
Forces (N)	27 km	2740	1113	3853
Mot-off	31.9 km	1367	548	1915

In order to verify the effect of the chemical scheme for air-hydrogen combustion, an additional analysis has been done considering a simplified configuration of only the internal flow path (see Figure 9) and a more detailed chemical scheme (Jachimowski with 9 species and 12 reactions).

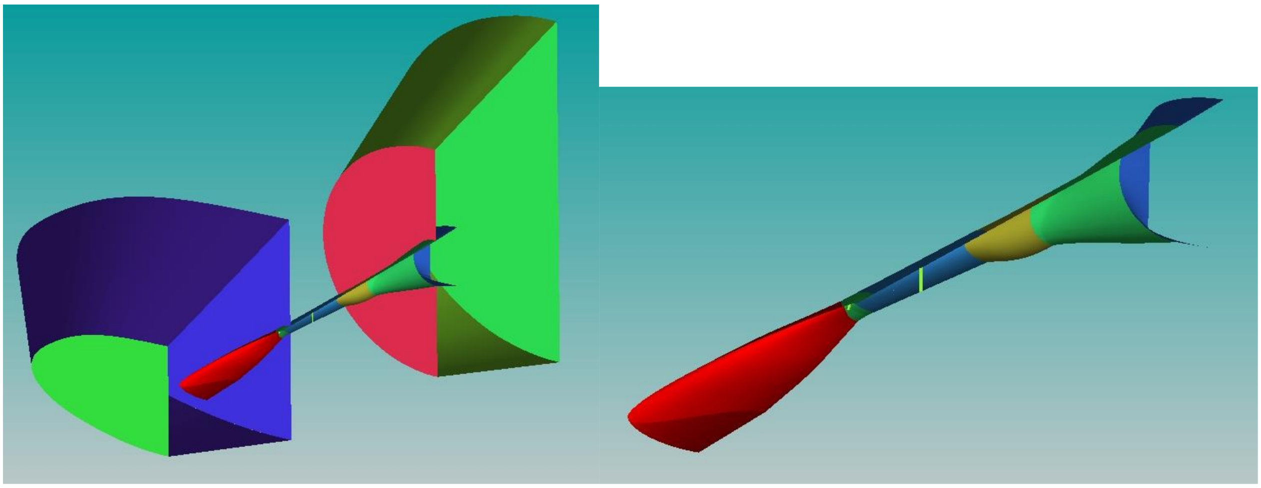

Figure 9: Internal flow path configuration.

Table 6: Summary of axial forces acting on the hypersonic propelled demonstrator

	Domain	CD_intake	CD_struts	CD_comb_nozzle	CD_all_int	F_comb_nozzle	F all int
Mono-st	whole	0.005221652	0.00146725	-0.015839459	-0.009151	-2624	-1516
Mono-st	internal	0.003486158	0.00274239	-0.016867853	-0.010639	-2795	-1763
Jachi	internal	0.003509144	0.00264422	-0.015555827	-0.009402	-2577	-1558

Main results are reported in Table 6 and can be summarized as follows:

- Good comparison between whole domain (NS) and internal domain (EUL) for what concerns the net thrust (all internal flow path). 1516 vs 1763 N
- Reduction of about 11% of net thrust (all internal path) using a more detailed chemical scheme. 1763 N → 1558 N
- Reduction of about 8% of gross thrust (combustor and nozzle) using a more detailed chemical scheme. 2795 N → 2577 N.

The reduction of the thrust should be in any case compensated with a higher ER (i.e., by injecting more fuel).

DOI: 10.13009/EUCASS2023-903

5. Aerodynamic Database

This section describes the operations performed in order to obtain the Aerodynamic Database (AEDB) for the hypersonic propelled demonstrator (Figure 3) which will be useful for conducting flight mechanics analyses ([8], [9], [10]).
The aerodynamic database is provided as a function of Mach number (M_{∞}), angle of attack (α) and the elevon deflections (δ_e) in *fuel-off* conditions. However, the analysis does not consider the effect of sideslip angle (β). The reference quantities are reported in Table 7. The Centre of Gravity is located at x_{CoG} = 2.33 m from the nose.

Table 7: Summary: Reference Quantities

Reference Length (L_{ref})	4.1248 m
Reference Surface (S_{ref})	4.7936 m^2
Mass	1120 kg
x_{CoG} range	2.30- 2.33 m

5.1 Clean Configuration

The aerodatabase of the SHEV vehicle has been completed for all the mission that foresees, after the ignition time (at least 10 seconds at constant altitude), a gliding aerodynamically controlled phase from Mach 7.35 to Mach 2.0, followed by a splash down on the sea. The CFD computations have been obtained running on the same grid of 7.6 million of cells and with the same turbulence model, but now in fuel-off conditions (see Table 8).
The test-matrix has been elaborated by scaling the X-43 Mach 7 flight profile to the hypersonic cruising altitude (Mach=7.35) of 27 km. A sensitivity in fuel-on cruising conditions has been also performed by adding ±2deg to AoA=0 deg at M=7.35 while a range from -4° to +4° for the AoA in fuel-off ones has been considered. The fuel-off descent, based on the estimated preliminary trajectory, needs to be verified downstream in the analysis of Flight-Mechanics. The AEDB data is released with increasing reliability for flight mechanics analysis and trajectory calculation in the framework of the project.

Table 8: Test Matrix for CFD computations

h (km)	Mach	AoA	engine	P	Temp	Dens	a	Vel	mu
27.00	7.35	-2, 0, 2, 4	fuel-off/on	1847.46	223.65	0.028777	299.799	2203.52	1.47164E-05
26.19	7	-2, 0, 2, 4	fuel-off	2091.26	222.84	0.032693	299.255	2094.79	1.46711E-05
25.25	6	-2, 0, 2, 4	fuel-off	2416.16	221.90	0.037932	298.623	1791.74	1.46324E-05
23.36	5	-2, 0, 2, 4	fuel-off	3236.22	220.01	0.051243	297.349	1486.75	1.45123E-05
20.54	3.5	-2, 0, 2, 4	fuel-off	5028.52	217.19	0.080656	295.437	1034.03	1.43532E-05
17.72	2	-2, 0, 2, 4	fuel-off	7843.63	216.65	0.126124	295.070	590.14	1.43226E-05

Looking at the following figures (from Figure 10 to Figure 12) we can deduce that:

- Linear trend of CL for full vehicle (External + Internal) except in fuel-on (M=7.35) where there is a decrease of the derivative CL_{α} with increasing of AoA.
- Quadratic trend of CD. At M=7.35 fuel-on the aero-propulsive balance is “negative” at AoA=2° that means that the external drag is greater than the “net thrust” of the internal flow path. This is due to the fact that at higher angle of attack the intake captures less air and so the scramjet engine gives a lower “thrust”. The opposite can be observed at AoA=-2° where there is a higher mass flow rate and thrust.
- In the gliding phase from M=7.35 to M=2.00 an out of trend of CL can be observed (see Figure 12). At M=3.5 the CL is lower than expected. This is due to the expulsion of the shock waves train from combustor duct, and the consequent positioning of the shock wave over the intake giving a local down-lift.
- The external coefficients are all regular as expected from linear aerodynamics. There is no influence of the shock wave train positioning along the gliding trajectory.
- From the internal coefficients we can see, as expected from previous considerations, great values of drag and down-lift at M=2.00, 3.50 (expulsion of shock waves train), small values for other Mach number and in particular negative drag (that means positive internal thrust) at M=7.35 Fuel-On.

DOI: 10.13009/EUCASS2023-903

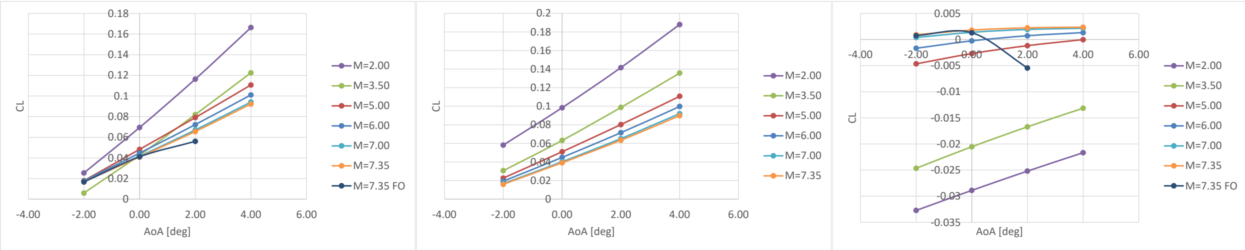

Figure 10: Lift Coefficient: Full vehicle, External part, Internal part.

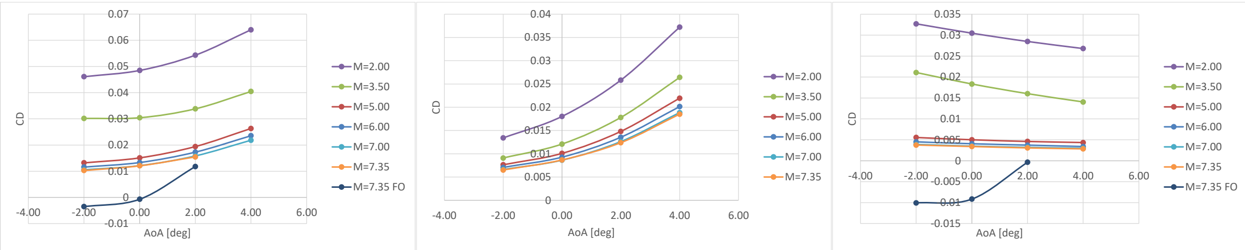

Figure 11: Drag Coefficient: Full vehicle, External part, Internal part.

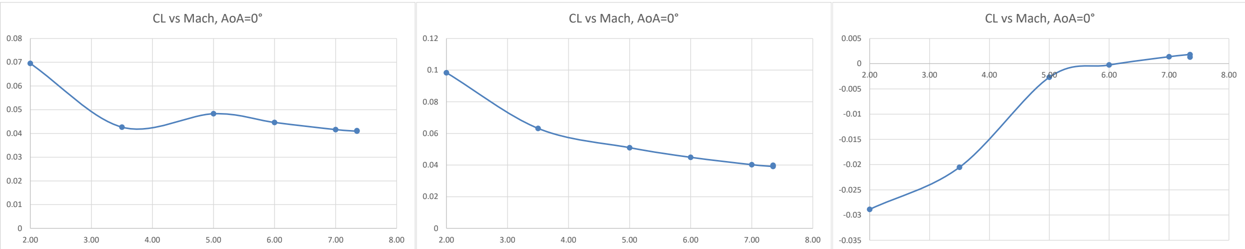

Figure 12: Lift Coefficient at AoA=0°: Full vehicle, External part, Internal part.

5.2 Control Surfaces Effect

The aerodatabase with considering the deflection of control surfaces (i.e., the elevons) is reported in this section. The variation of the aerodynamic coefficients is assessed as the difference between the aerodynamic coefficients of the configuration evaluated with deflected elevon and the coefficients evaluated with the undeflected elevon (e.g., $\Delta \boldsymbol{C_M}(\boldsymbol{\delta_e}) = C_{M_{\delta_e}} - C_{M_{\delta_e=0}}$).
In order to obtain this, a simplified configuration constituted of the wing and elevon has been considered (Figure 13) with an inviscid flow hypothesis.
The following ranges have been analysed to generate the longitudinal aerodynamic data sets:

- $2 \leq M_\infty \leq 7.35$
- $-2° \leq \alpha \leq 4°$
- $-20° \leq \delta_e \leq 10°$

The Pitching Moment Coefficient of the flapped wing is reported in Figure 14.

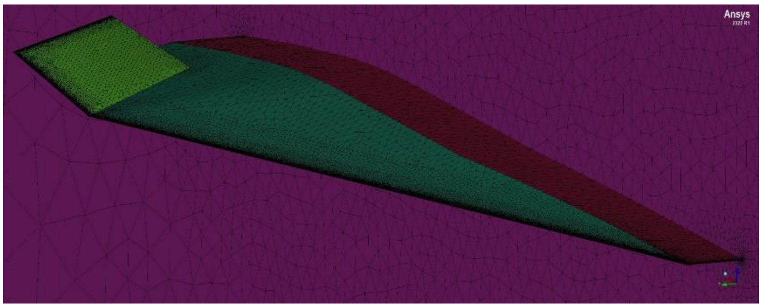

Figure 13: Grid for a stand-alone wing with a deflected elevon.

DOI: 10.13009/EUCASS2023-903

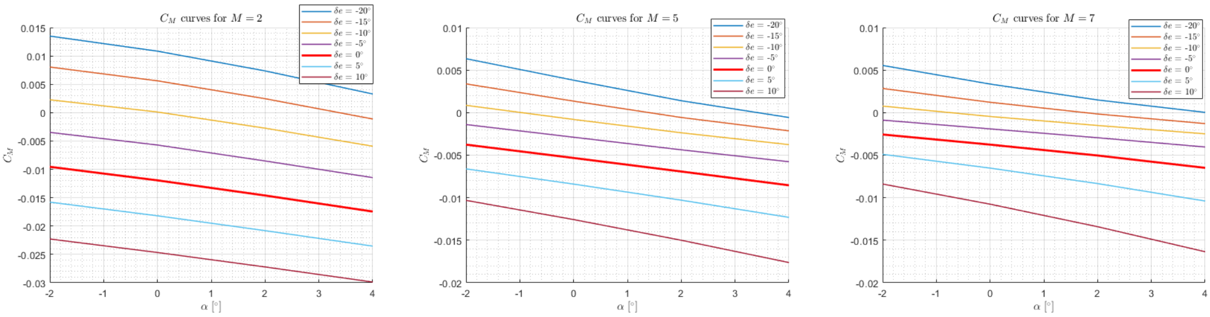

Figure 14: Effect of Flap Deflection on Pitching Moment Coefficient.

As final step we report the complete aerodynamic database, i.e., the database of the hypersonic propelled demonstrator configuration that considers also the effect of control surfaces (elevons). Figure 15, Figure 16 and Figure 17 show, respectively, the lift, drag and pitching moment coefficient distributions in function of AoA for three different elevon deflections (from -20°, -5°, +10°) and Mach numbers (from 2.0 to 7.35). Please, note that the pitching moment is evaluated with respect to X_{CoG}=2.3099 m.

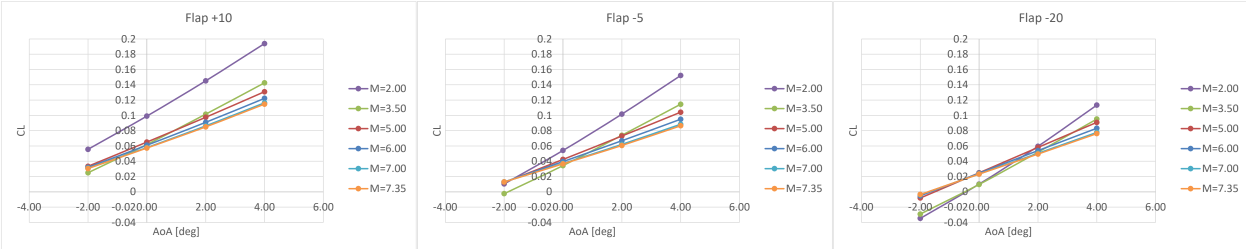

Figure 15: Lift Coefficient at three different elevon deflections.

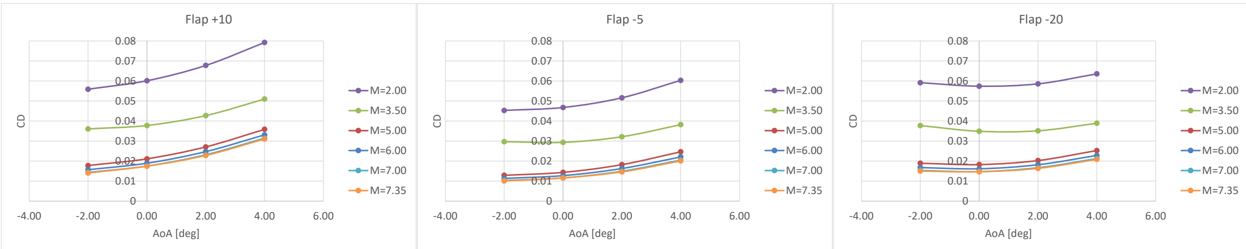

Figure 16: Drag Coefficient at three different elevon deflections.

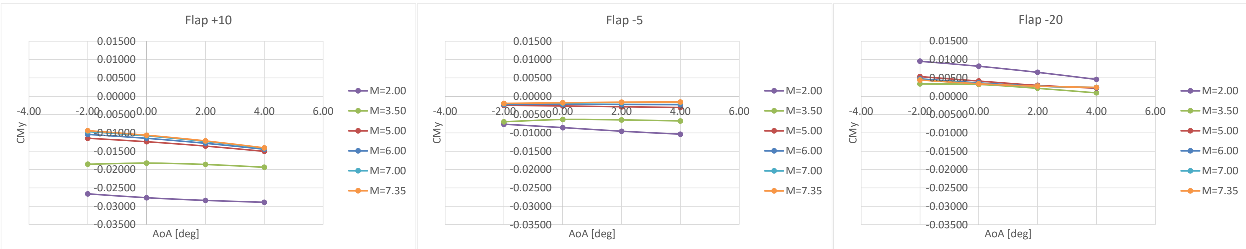

Figure 17: Pitching Moment Coefficient at three different elevon deflections.

5. Conclusions

This paper reports the first results of the AEDB characterization for the SHEV vehicle obtained mainly from CFD viscous and reacting simulations. The final AEDB will also take into account the experimental data results whose activity is going to start. The main results can be summarized as follows:

- Positive aero-propulsive balance for two possible mission points, with a lower net thrust (as a percentage of total drag) at higher altitude due to the lower Reynolds number (higher viscous effects).
- Slight effect of altitude on Eulerian reactive simulations due to different asymptotic conditions of pressure and temperature (different hydrogen input conditions, chemical effect).

DOI: 10.13009/EUCASS2023-903

- Viscosity effect on engine performance: improved combustion efficiency due to better mixing, however viscous resistance is added.
- Sensitivity conducted for chemical modelling of air-hydrogen combustion on internal flowpath (Intake-Combustor-Struts-Nozzle). The use of the multi-step "reduced-Jachimowsky chemical model" showed, compared to the mono-step, a reduction in gross thrust (Combustor and nozzle) of about 8% and in net thrust of about 11%.
- First version of the SHEV vehicle (demonstrator) aerodynamic database (AEDB) in the range of Mach = 7.35 – 2.00. The AEDB is based on CFD viscous calculations for the clean configuration and on CFD inviscid ones for the control surface effect. The AEDB has been provided to Flight Mechanics team for stability, trimmability and controllability analysis and trajectory calculations.

Starting from the consolidated AEDB and trajectory analysis, next activities will focus on the maturation of the demonstrator design and on the selection of materials, together with the definition of test campaign on a subscale model.

Acknowledgements

The work has been funded by Italian Space Agency and CIRA ScpA in the frame of the agreement nr. 2022-13-HH.0 -F43D22000410005.

References

[1] J. Steelant, R. Varvill, C. Walton, S. Defoort, K. Hannemann, M. Marini, "Achievements Obtained for Sustained Hypersonic Flight within the LAPCAT-II Project", AIAA-2015-3677, 20th AIAA International Space Planes and Hypersonic Systems and Technologies Conference, July 06-09, 2015.

[2] E. Blanvillain, G. Gallic, "HIKARI: Paving the way towards High Speed Air Transport", AIAA-2015-3676, 20th AIAA International Space Planes and Hypersonic Systems and Technologies Conference, July 6-9, 2015.

[3] Mack A., Steelant J., Adirim H., Lentsch A., Marini M., Pilz N., "FAST20XX: Achievements on European Suborbital Space Flight", 7th European Symposium on Aerothermodynamics, Brugge, Belgium, May 2011.

[4] J. Steelant et al., "Achievements obtained within ATLLAS-II on Aero-Thermal Loaded Material Investigations for High-Speed Vehicles", 21st AIAA International Space Planes and Hypersonics Technologies Conference, 6-9 March 2017, China.

[5] J. Steelant et al., "Conceptual Design of the High-Speed Propelled Experimental Flight Test Vehicle HEXAFLY", AIAA-2015-3539, 20th AIAA International Space Planes and Hypersonic Systems and Technologies Conference, Glasgow, Scotland, U.K., July 6-9, 2015.

[6] G. Pezzella, M. Marini, M. Cicala, A. Vitale, T. Langener, J. Steelant, "Aerodynamic Characterization of HEXAFLY Scramjet Propelled Hypersonic Vehicle", AIAA-2014-2844, AIAA Aviation, 32nd AIAA Applied Aerodynamics Conference, 16-20 June 2014, Atlanta, GA, USA.

[7] Di Benedetto S., Di Donato M.P., Schettino A., Scigliano R., Nebula F., Morani G., Cristillo D., Marini M., Cardone S., Steelant J., Villace V., "The high-speed experimental flight test vehicle of HEXAFLY-INT: a multidisciplinary design",CEAS Space Journal, published online on 5 January 2021, DOI: 10.1007/s12567-020-00341-5.

[8] Viola N., Fusaro R., Saracoglu B., Schram C., Grewe V., Martinez J., Marini M., Hernandez S., Lammers K., Vincent A., Hauglustaine D., Liebhardt B., Linke F., Fureby C., "Main Challenges and Goals of the H2020 STRATOFLY Project", Aerotecnica Missili & Spazio (2021) 100:95–110, Published online: 29 May 2021, https://doi.org/10.1007/s42496-021-00082-6.

[9] Roncioni P., Vitagliano P. L., De Gregorio F., Pezzella G., Romano L., Paglia F.," Aerodynamic Appraisal of the VEGA-C Launcher", JSR-Journal of Spacecraft and Rockets, 24 April 2023, http://arc.aiaa.org | DOI: 10.2514/1.A35610.

[10] Viola N, Roncioni P., Gori O., Fusaro R., "Aerodynamic Characterization of Hypersonic Transportation Systems and Its Impact on Mission Analysis", MDPI-Energies, 16 June 2021, https://doi.org/10.3390/en14123580.

[11] System engineering general requirements, ECSS-E-ST-10C.

[12] Technical requirements specification, ECSS-E-ST-10-06C.

[13] S. Defoort, L. Serre, R. Grenon, Narmada, "ZEHST: Environmental challenges for hypersonic passenger transport", AIAA 2012-5873, 18th AIAA/3AF International Space Planes and Hypersonic Systems and Technologies Conference, September 2012.

[14] U. Mehta, M. Aftosmis, J. Bowles, S. Pandya, "SKYLON Aerodynamics and SABRE Plumes", AIAA 2015-3605, 20th AIAA International Space Planes and Hypersonic Systems and Technologies Conference, Glasgow, Scotland, U.K., July 6-9, 2015.